CHALMERS
UNIVERSITY OF TECHNOLOGY

Reconstruction of a Global Transcriptional Regulatory Network for Control of Lipid Metabolism in Yeast by Using Chromatin

AMERICAN SOCIETY FOR MICROBIOLOGY | mSystems®

RESEARCH ARTICLE
Molecular Biology and Physiology

Reconstruction of a Global Transcriptional Regulatory Network for Control of Lipid Metabolism in Yeast by Using Chromatin Immunoprecipitation with Lambda Exonuclease Digestion

David Bergenholm,[a] Guodong Liu,[a]* Petter Holland,[a] Jens Nielsen[a,b]

[a]Department of Biology and Biological Engineering, Novo Nordisk Foundation Center for Biosustainability, Chalmers University of Technology, Gothenburg, Sweden

[b]Novo Nordisk Foundation Center for Biosustainability, Technical University of Denmark, Hørsholm, Denmark

ABSTRACT To build transcription regulatory networks, transcription factor binding must be analyzed in cells grown under different conditions because their responses and targets differ depending on environmental conditions. We performed whole-genome analysis of the DNA binding of five *Saccharomyces cerevisiae* transcription factors involved in lipid metabolism, Ino2, Ino4, Hap1, Oaf1, and Pip2, in response to four different environmental conditions in chemostat cultures, which allowed us to keep the specific growth rate constant. Chromatin immunoprecipitation with lambda exonuclease digestion (ChIP-exo) enabled the detection of binding events at a high resolution. We discovered a large number of unidentified targets and thus expanded functions for each transcription factor (e.g., glutamate biosynthesis as a target of Oaf1 and Pip2). Moreover, condition-dependent binding of transcription factors in response to cell metabolic state (e.g., differential binding of Ino2 between fermentative and respiratory metabolic conditions) was clearly suggested. Combining the new binding data with previously published data from transcription factor deletion studies revealed the high complexity of the transcriptional regulatory network for lipid metabolism in yeast, which involves the combinatorial and complementary regulation by multiple transcription factors. We anticipate that our work will provide insights into transcription factor binding dynamics that will prove useful for the understanding of transcription regulatory networks.

IMPORTANCE Transcription factors play a crucial role in the regulation of gene expression and adaptation to different environments. To better understand the underlying roles of these adaptations, we performed experiments that give us high-resolution binding of transcription factors to their targets. We investigated five transcription factors involved in lipid metabolism in yeast, and we discovered multiple novel targets and condition-specific responses that allow us to draw a better regulatory map of the lipid metabolism.

KEYWORDS ChIP-exo, transcriptional regulatory network, environmental response, lipid metabolic map, novel targets

Cellular functions are reprogrammed in response to environmental changes, and transcription factors (TFs) play a key role in this regulation. The complexity of transcriptional regulation in eukaryal cells and the lack of knowledge regarding the structure of regulatory networks, however, limit understanding of how this type of reprogramming occurs. Approximately 200 sequence-specific TFs have been characterized or predicted in the model organism *Saccharomyces cerevisiae* (1). In transcriptional regulatory systems of low connectivity (such as that in *Escherichia coli* [2–4]) or in systems that have hierarchical structures, TF deletion studies have proved to be useful, as the resulting phenotype corresponds well with the function of the deleted TF.

Received 15 December 2017 **Accepted** 4 July 2018 **Published** 31 July 2018

Citation Bergenholm D, Liu G, Holland P, Nielsen J. 2018. Reconstruction of a global transcriptional regulatory network for control of lipid metabolism in yeast by using chromatin immunoprecipitation with lambda exonuclease digestion. mSystems 3:e00215-17. https://doi.org/10.1128/mSystems.00215-17.

Editor Paul Wilmes, Luxembourg Centre for Systems Biomedicine

Address correspondence to David Bergenholm, david.bergenholm@chalmers.se, or Jens Nielsen, nielsenj@chalmers.se.

* Present address: Guodong Liu, School of Life Science, Shandong University, Jinan, China.

D.B. and G.L. are co-first authors.

However, in *S. cerevisiae* where a hierarchical structure of transcription factors does not exist due to the complex regulation with internal loops where TFs are controlling each other (5) and where genes are regulated by multiple TFs, deletion of individual TFs followed by genome-wide transcription analysis has not allowed us to identify the full function of TFs (6). To better resolve these combinatorial regulations and internal regulatory loops, it is necessary to identify the binding sites of transcription factors at a high resolution and their changes in response to environmental conditions. Here we demonstrate that by using this approach, it is possible to reconstruct a transcriptional regulatory network for lipid metabolism in yeast by mapping binding of five TFs that are involved in regulation of lipid metabolism: Ino2, Ino4, Hap1, Oaf1, and Pip2.

To generate a genome-wide lipid metabolic transcriptional regulatory network, we used chromatin immunoprecipitation with lambda exonuclease digestion (ChIP-exo) (7), followed by high-throughput sequencing, to map binding of these five TFs. Earlier studies on the genome-wide binding of these TFs were done mainly in rich media using chromatin immunoprecipitation with microarray technology (ChIP-chip) (8), which does not allow the precise binding sites to be mapped or evaluation of conditional binding under different conditions. The use of different culture conditions to map differential binding of TFs has been suggested (9), and recently, we showed that this allowed the identification of new functions of the transcription factor Cst6 (10).

Ino2, Ino4, Hap1, Oaf1, and Pip2 all play important roles in the lipid metabolic network of *S. cerevisiae*. Ino2 and Ino4 are paralogues that belong to the basic helix-loop-helix (bHLH) family and form a heterodimer that is involved in the phospholipid biosynthetic pathway (11). The YeTFaSCo database gives the consensus DNA-binding motif for the two TFs as CACATGC (12), which is also called the UAS_{INO} motif (13). Single deletions of either Ino2 or Ino4 yielded a decrease in phospholipid biosynthesis relative to the wild type, whereas the two regulators also have some different targets according to the transcriptome analysis (14). Hap1 is a Zn_2Cys_6 zinc finger TF that responds to oxygen and heme levels. Heme acts as an activator for Hap1 and the expression of the Rox1 repressor, and together, they form a circuit that fine-tunes the control of the oxygen-responsive pathways (15). The previously reported consensus motif for Hap1 is CCGXTAXXXCCG (16). Oaf1 and Pip2 are also C_6 zinc finger TFs involved in β-oxidation and peroxisomal biogenesis, which can act as a heterodimer to bind oleate-responsive elements (OREs) (17), but they can also act independently of each other (18). The previous reported consensus motif for the Oaf1-Pip2 heterodimer is CGGXXXTX(7–10)CCG (19).

In our study we used chemostat cultures to generate chromatin binding data because this allows the analysis to be performed under well-controlled growth conditions and operation under different environmental conditions at the same specific growth rate. Four different limited conditions regarding different nutrition and oxygen availabilities were used to cover a wide range of different environmental growth conditions for *S. cerevisiae*.

RESULTS

Chemostat cultures and ChIP-exo mapping. Strains expressing each of the five transcription factors (TFs) were constructed to have an *in situ* C-terminal tandem affinity purification (TAP) tag to enable immunoprecipitation of the TF. Each strain was cultured in chemostats with different limiting conditions in biological duplicates: nitrogen (N-lim), glucose (Glu-lim), glucose and oxygen (Ox,Glu-lim), and ethanol (Et-lim). Samples from each chemostat experiment were used to cross-link and purify DNA-protein complexes and digest nucleotides not covered by the cross-linked protein by the ChIP-exo method. Following release from the DNA-protein complex, the DNA was sequenced, and the reads were aligned to the reference genome assembly R64-2-1 of *S. cerevisiae* S288C. The identified TF-binding events were assigned to the closest gene and further analyzed for their biological impacts.

ChIP-exo identified high-resolution targets of the five TFs. The binding events from the ChIP-exo experiments with each TF were analyzed with the peak-finding

algorithm GEM (20). The identified events were then assigned a binding ratio, which corresponds to the signal-to-noise ratio (*S*/*N*), where the duplication showed a good correlation (see Fig. S1 in the supplemental material). ChIP-exo identified the binding positions of the TFs on target promoters with high resolution, which can be visualized for all five of the studied TFs (Fig. 1A). The reads from all events found were extracted 300 bp before and 300 bp after each event. The events were then aligned at the center to create a heat map of binding profiles, as shown in Fig. 1B. From these results, it is observed that the binding profiles of Ino2, Ino4, Oaf1, and Pip2 are narrow, whereas Hap1 has a broader binding profile. The broader binding of Hap1 seems to be a result of CCG/GCG-rich regions. Investigating the distribution of binding events on the promoter regions showed that 60 to 80% of all binding occurs within the 600 bp upstream of the ATG codon (Fig. S2). By investigating the promoter regions of identified genes, we found that many promoters have multiple binding sites for one TF (Fig. 1C). An example of such multiple binding is demonstrated in Fig. 1D, where Ino2 bound to three sites in the promoter of *CHO2*. The binding sequences for Ino2 in the *CHO2* promoter are not directional, and none of the identified binding sites have the exact above-mentioned Ino2 consensus motif.

We further compared all the identified targets for each TF (listed in Tables S1 to S5 in Data Set S1 in the supplemental material) to those identified in a previous ChIP-chip study where yeast was grown unlimited in rich media (9) (Fig. 1E). For Ino2 and Ino4, we confirmed most of the previously reported targets but also found hundreds of new targets. For Hap1, 143 targets overlapped with the targets of previous reports in the literature, although we missed 72 targets that had previously been reported, possibly due to the different culture conditions used or decreased significance of some peaks after data treatment (Fig. S3). For Oaf1 and Pip2, only a few targets overlapped with the previous ChIP-chip data. Oaf1 and Pip2 targets identified earlier by ChIP-chip are, however, questionable, as they did not identify most of the β-oxidation genes that are known Oaf1-Pip2-binding targets as evidenced by other studies (21) and our study (Table S8 in Data Set S1). Of the 85 oleate-responsive elements (OREs) previously predicted in putative promoter regions (18), 38 were identified to be bound targets of Oaf1 or Pip2. Combining the binding sites detected by us and the 15 ones identified previously (22), we expand the bound ORE targets for Oaf1 or Pip2 to 45.

Because all the studied TFs are involved in lipid metabolism, some overlap between their targets was expected. Specifically, 35 genes were found to show binding of all five TFs (Fig. 2A), including seven genes involved in lipid metabolism. The overlapping targets for each condition are displayed in Fig. S4. Some of the shared targets are displayed in Fig. 2B, which shows the binding of three TFs on the promoter of *OLE1* encoding delta-9 fatty acid desaturase. The binding is highly concentrated in the same region. Looking closer at this region reveals that two binding motifs of Hap1 surrounded the binding sites of Oaf1 and Ino2, constituting a highly optimized region for responses to different signals, including oxygen levels, fatty acids, and membrane composition. This region overlaps with a previously reported region that has been called the fatty acid-responsive element (FAR) (23). With our data, we can now show which TF is responsible for the FAR. Figure 2B also displays the binding of three TFs on the promoter of *ERG11* encoding sterol 14-demethylase, where the binding sites are dispersed throughout the promoter region.

New insights into the consensus binding motifs. We studied the motifs of binding sequences for each TF under each condition using the GEM software and then the MEME suite. The consensus motifs are displayed in Fig. 3A. For Ino2 and Ino4, the consensus motif found was CACATGC, which is the previously reported consensus motif in the YeTFaSCo database (12). The consensus motifs of Hap1 were found to be variations of the previously reported consensus motif CCGXTAXXXCCG. For N-lim and Et-lim, CCGXTATXTCC was found to be the consensus motif, and for Ox,Glu-lim and Glu-lim, the consensus motif was CCGATA. For Oaf1, CGGXXXTAA was found as a consensus motif under all conditions where the previously reported motif was CCGXXX-

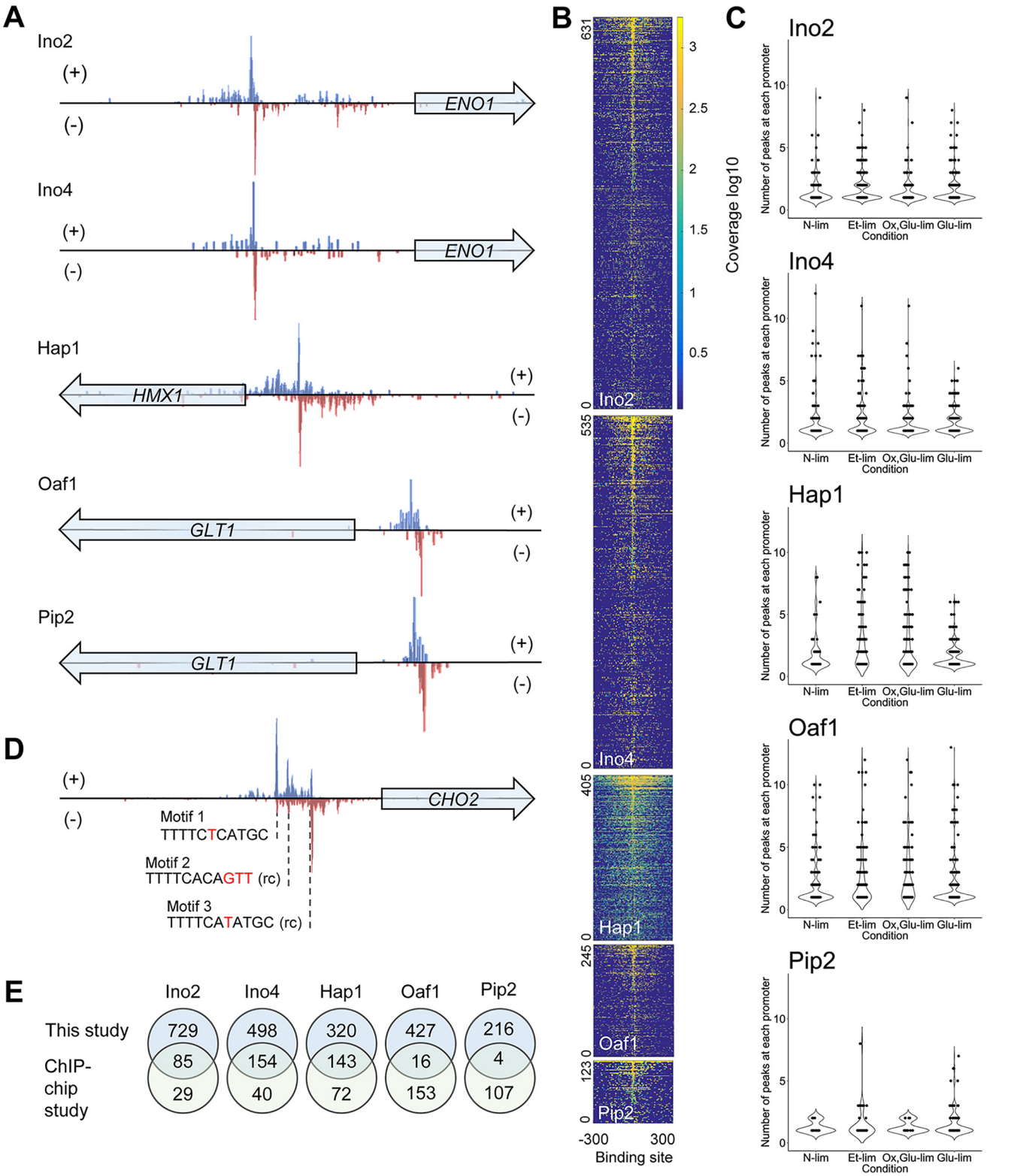

FIG 1 Identification of direct target genes of TFs by ChIP-exo. (A) Examples of TF-binding sites identified at high resolution. The distribution of 3′-trimmed sequencing reads mapped to forward (+) and reverse (−) strands of gene promoters are shown. (B) Heat map showing the binding of TFs on all target regions under the glucose-limited (Glu-lim) condition. Coverage values indicate the counts of reads around the center of binding sites. For each TF, the rows representing binding events are sorted by *S/N* ratio and aligned to their centers. (C) Violin plots of each TF and their peak count for each promoter. Most promoters have one or two binding sites per TF, but there can be even higher numbers. (D) Multiple binding sites of Ino2 on the promoter of *CHO2* under Et-lim condition. Three binding motifs of Ino2 are shown with sequence variations relative to the consensus motif (CACATGC) colored in red. rc, reverse complement sequence. (E) Comparison of the target genes encoding proteins under four conditions identified in this study and those in the previous ChIP-chip study with rich media (9). For the ChIP-chip data, genes with *P* value of <0.01 in the original data set are considered significant targets.

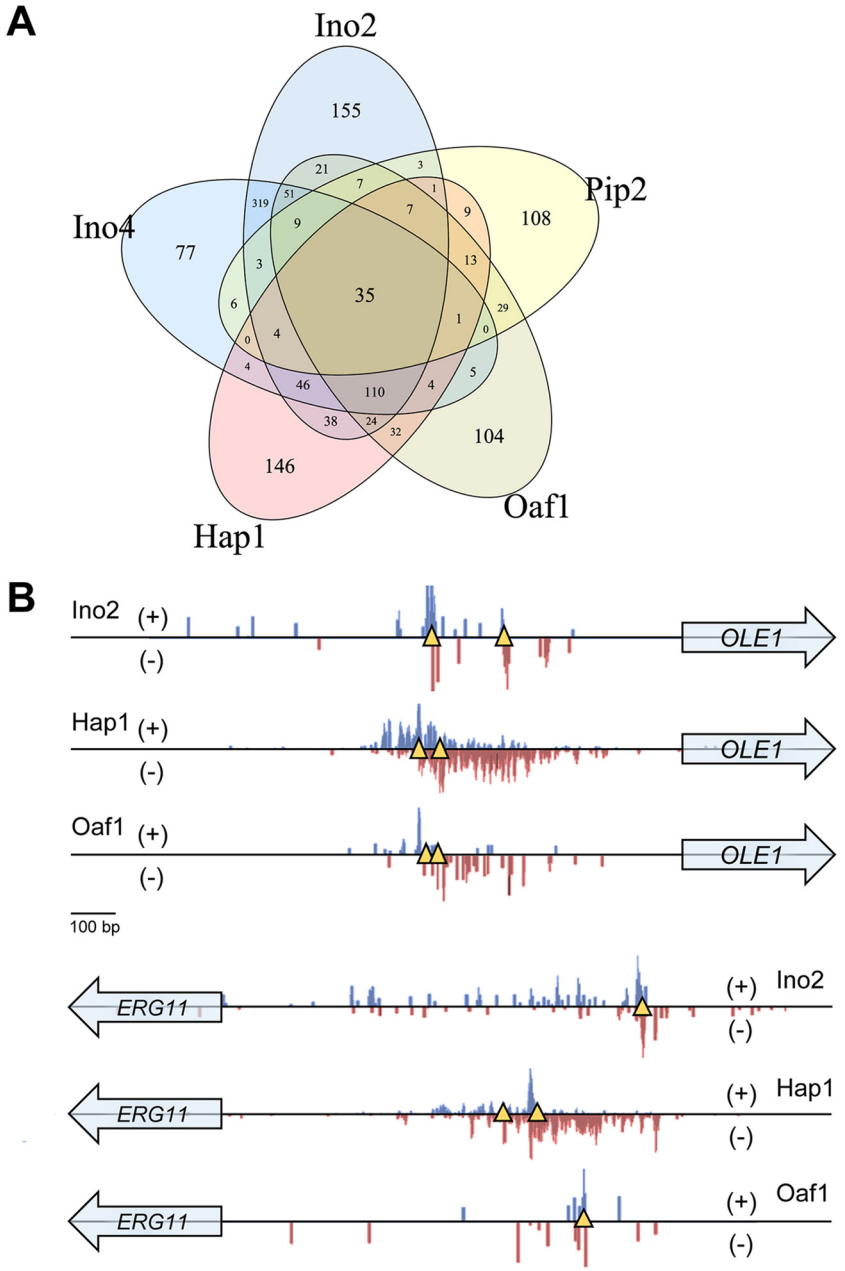

FIG 2 Combinatorial binding of TFs on target genes. (A) Venn diagram showing overlap of all the target genes of the five TFs. (B) Binding of Ino2, Hap1, and Oaf1 on the promoters of *OLE1* and *ERG11* under the Glu-lim condition. The distribution of 3′-trimmed sequencing reads mapped to forward (+) and reverse (−) strands of gene promoters are shown. Yellow triangles indicate putative binding sites of the corresponding TF according to the known consensus motif.

TXA. For Pip2, the previously reported motif is the same as for Oaf1. Here it was found that Pip2 has CCGXXXTA as a consensus motif under all conditions but with more variation at the four to six positions.

We calculated the distribution of binding ratio (*S*/*N*) and the number of binding events identified for each k-mer group in motif discovery. As seen in Fig. 3B (data for Ino2 at Glu-lim), we could not identify a distinction between 7-mer groups in binding ratio. There was, however, a preference toward two of the 7-mers, TCACATG and CACATGC, which account for ~41% of all binding events found. For N-lim, Ox,Glu-lim, and Et-lim, the two most common 7-mers account for 74%, 38%, and 57% of all binding

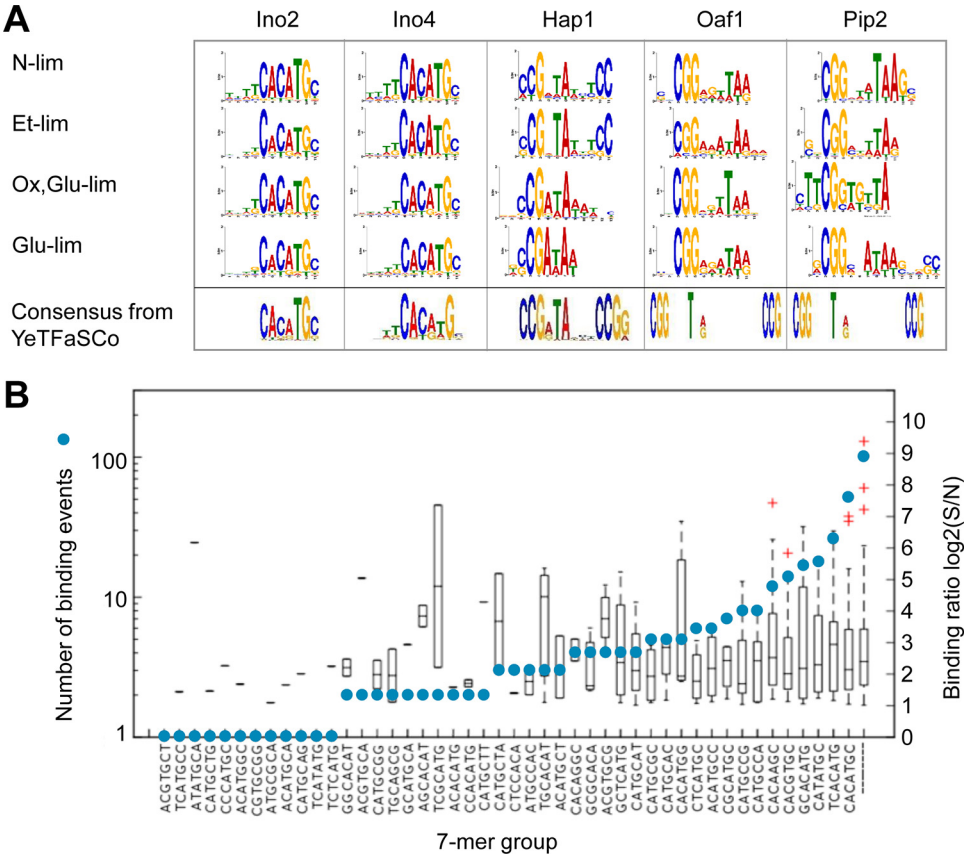

FIG 3 Consensus binding motifs of TFs. (A) Sequence logos of consensus motifs under different conditions. The motifs were identified using the MEME algorithm. Consensus motifs of the highest score for each TF in the YeTFaSCo database are shown for comparison. (B) Binding sequences of Ino2 under the Glu-lim condition. Blue circles show the numbers of binding events containing the indicated specific 7-mer sequence. Box plots show the binding levels of the events containing the sequence. For binding events containing multiple 7-mer sequences (e.g., TCACATGC containing both TCACATG and CACATGC), only the 7-mer with the most significant enrichment was counted.

events, respectively. Similar trends were observed for all the TFs and their consensus motif under all conditions.

Condition-dependent binding. The different number of binding targets as well as altered occupancy levels in response to environmental changes were clearly observed for the five TFs (Tables S1 to S5 in Data Set S1). We investigated the overlap of gene targets between the conditions for each TF (Fig. 4A). Some gene targets are common for all conditions, which could be seen as a "core set" of gene targets. However, the interesting part is the shift of targets between conditions and thus their response to environmental changes. While constitutively binding to some targets (e.g., *CHO2* for Ino2 and *EEB1* for Pip2), Ino2 and Pip2 bind to additional targets (e.g., *PCT1* for Ino2 and *MDH2* for Pip2) only under respiratory metabolic conditions (Fig. 4B), resulting in higher number of targets under the latter conditions. This connection between metabolic states and TF binding indicates that the TFs have different biological functions by altering their targets in response to specific environmental or physiological signals.

One explanation for the differential binding could be different expression levels of the TFs under different conditions. However, the transcription level of each TF does not correlate with the number of targets identified for each condition (Fig. S5). This indicates that the range of targets is highly controlled by several factors such as posttranslational modifications of TFs and also chromatin structure (such as nucleosome occupancy) having an influence on the availability of targets for the TFs. The binding of Ino2 or Ino4 (Ino2/4) on a hexose transporter gene-enriched region provides

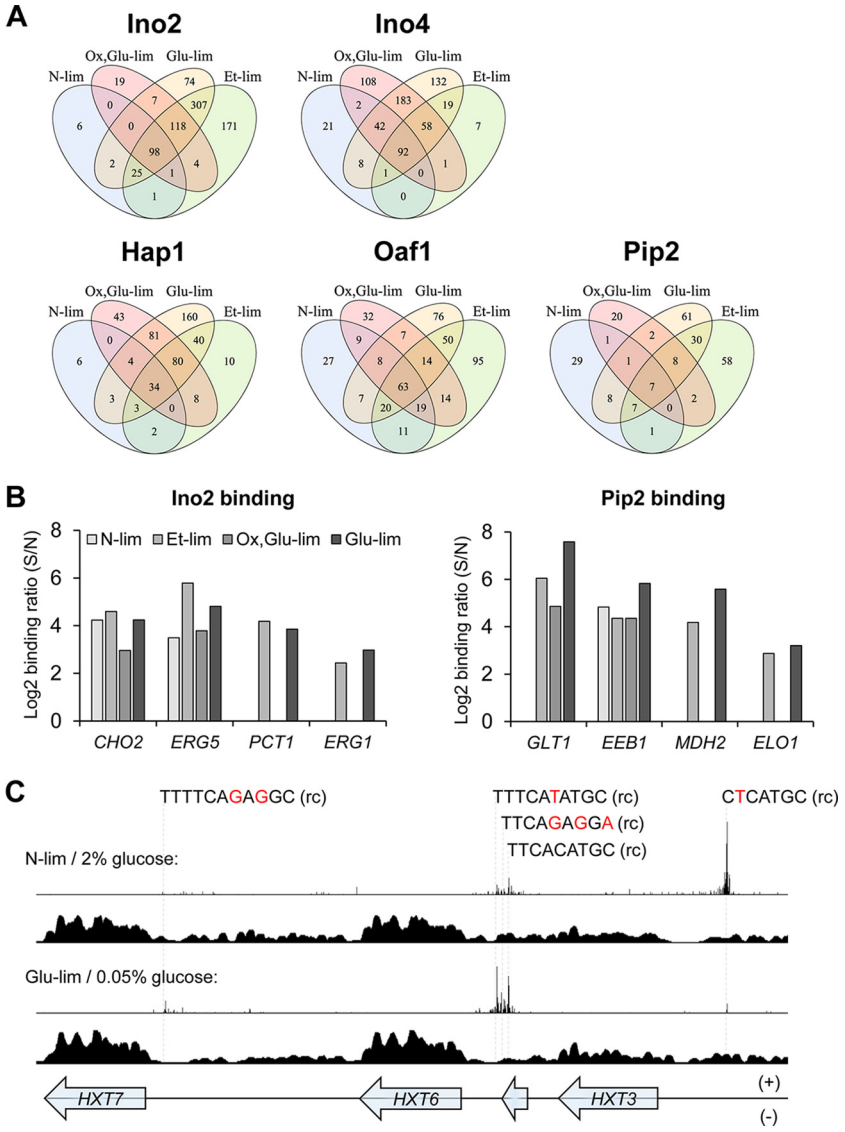

FIG 4 Growth condition-dependent binding of TFs. (A) Venn diagram of the TF targets and their overlap between conditions. Several genes for each TF are independent of the condition; however, many more genes are condition specific. (B) Differential binding of Ino2 and Pip2 on the promoter regions of specific target genes under different conditions. Binding ratios with $\log_2$ value below 1 are filtered out in data processing and are not shown. (C) Hexose transporter gene-rich region bound by Ino4 and nucleosomes under different conditions. For each group of conditions, the distributions of 3′-trimmed ChIP-exo reads of Ino4 (top plot) and sequencing reads of nucleosome-occupying regions (nucleosome-seq) (bottom plot [data from reference 24]) are shown. For nucleosome-seq data, cells were cultivated in synthetic complete medium containing 2% or 0.05% glucose, and DNA regions covered by sequencing reads indicate nucleosome-occupying regions. Sequence variations of binding sites relative to the consensus motif of Ino4 (CACATGC) are colored in red. rc, reverse complement sequence.

some clues for the latter hypothesis. As shown in Fig. 4C, the promoters of hexose transporter genes *HXT3*, *HXT6*, and *HXT7* are occupied differently under N-lim and Glu-lim conditions by Ino4 (similar findings for Ino2 [data not shown]). We overlaid nucleosome distribution data adapted from reference 24, and even though the culture conditions are not completely the same in the two studies, the data integration makes sense from the aspect of glucose supply, and the results are striking. During growth at 2% glucose (glucose fermentation), the chromatin structure at the precise site of Ino2/4 binding is open at the *HXT3* site, whereas for *HXT6* and *HXT7*, the chromatin at the corresponding sites is closed. The opposite behavior can be observed during growth at 0.05% glucose (glucose respiration). This difference in chromatin structure is consistent

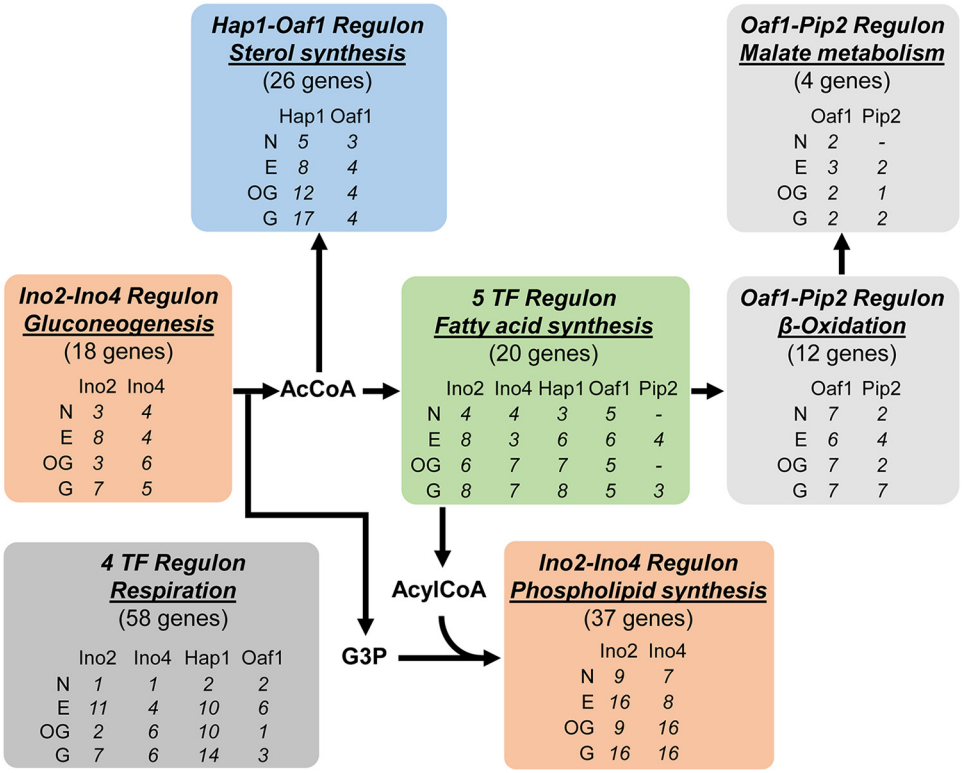

FIG 5 Coordination of lipid metabolism-related processes by TFs. The biological processes reported to have statistical significance (*P* value < 0.01) in gene set analysis of target genes with binding ratio $\log_2(S/N)$ of >1 are shown. For a TF(s) significantly associated with a certain process, the number of bound genes is shown. A minus symbol indicates that the process is not significantly reported for the TF under the corresponding condition. Abbreviations of growth conditions: N, N-lim; E, Et-lim; OG, Ox,Glu-lim; G, Glu-lim.

with the different binding of Ino2/4 to this region between fermentative and respiratory metabolic conditions.

TF coordination of metabolic processes. To investigate the different biological processes and functions potentially regulated by the TFs, we used genome-wide gene ontology (GO) sets. For each TF, we ran a gene set analysis using the Piano R package (25). For input, we used the $\log_2(S/N)$ values and allowed GO terms that had *P* values of <0.01 to be selected as significant reporter terms (Fig. S6). While lipid metabolic process was confirmed as a significant target of all five TFs that we studied, many new functions were identified. For Ino2/4, we found that these TFs also bind genes in cell wall biogenesis and amino acid biosynthesis. The latter function was suggested in our previous study of *INO2*- or *INO4*-dependent genes through transcriptome analysis (14). Malate metabolism and glutamate biosynthesis, which are tightly connected to fatty acid utilization (26, 27), were identified as significant target processes of Oaf1 and Pip2.

Condition-dependent functions of the TFs were clearly revealed by the reporter GO term analysis of target genes. In line with the differential binding described above, Ino2 showed expanded binding under the respiratory metabolic conditions relative to the two fermentative metabolic conditions (Fig. S6). In addition to phospholipid biosynthesis as a constant target under all four conditions, Ino2 is associated with various processes, including cell wall biogenesis, methionine biosynthesis, and stress response under the respiratory metabolic conditions. Compared to Oaf1, the function of Pip2 targets is more affected by the culture conditions, with the highest number of reporter GO terms obtained under the Et-lim condition.

The differential functions of TFs in regulating specific metabolic processes were further studied by investigating their targets with binding ratios higher than $\log_2(S/N)$ of >1. Figure 5 summarizes the significant target processes related to lipid metabolism

obtained for each TF under each condition, where each individual binding target can be found in Table S9 in Data Set S1. Ino2 and Ino4 bind genes encoding proteins involved in glycolysis and gluconeogenesis, pathways providing acetyl coenzyme A (AcCoA) for both fatty acid and sterol syntheses and glycerol-3-phosphate (G3P) for phospholipid synthesis, as well as their well-known binding to genes encoding proteins involved in phospholipid synthesis. Hap1 binds sterol synthesis genes which utilize AcCoA, with Oaf1 also being involved under respiratory metabolic conditions. Ino2, Ino4, Hap1, Oaf1, and Pip2 all bind to fatty acid synthesis genes, providing substrates for phospholipid synthesis, indicating the tight regulation of this process in response to various upstream signals. To recycle fatty acids, Oaf1 and Pip2 bind β-oxidation genes producing peroxisomal AcCoA as well as coordinated malate and glutamate metabolism. Hap1 also has the highest number of binding targets among the five TFs within respiration.

Linking TF binding to transcriptional output and cellular lipid composition. The physical binding of a TF to a gene's promoter does not necessarily mean that it regulates the transcription level, due to the dose- and condition-dependent feature of transcriptional regulation (28). Thus, integration of the direct target set of a TF identified by ChIP-exo with the targets transcriptionally affected by that TF is beneficial to understanding its biological function (29). We previously determined transcriptome changes in mutants lacking *INO2* or *INO4* relative to the wild type for similar growth conditions as applied here (14). When revisiting these data, we found the transcription of some targets strongly occupied by Ino2, e.g., *INO1*, *FAS1*, and *OPI3*, to be markedly impaired by the deletion of *INO2* (Fig. 6A). However, other strong targets, e.g., *ACC1*, are only slightly affected in the deletion mutant, suggesting dominant regulatory roles of other TFs on these promoters. The transcription of *PHO84*, which is another target of Ino2, showed a surprising increase in the *INO2* deletion mutant. This "repressing" effect is in agreement with the results of a previous study of an *INO2* overexpression mutant (30), which could be explained by a unique feature of the Ino2 binding sequence on the *PHO84* promoter determined here to be GCACGTGG, -415 to -408 bp relative to the start codon. This sequence has a mismatch of one nucleotide from the Ino2 consensus motif, but it exactly matches the consensus binding motif of another TF, Pho4 (12), which might trigger competition between the TFs.

By integrating the ChIP-exo and transcriptome data of TF deletion studies, we were able to distinguish direct and indirect targets of Ino2 within Ino2-dependent genes (Fig. 6B). For the lipid metabolic genes described above, we found most phospholipid synthetic genes to be direct targets of Ino2 (Fig. S7). The binding strengths are generally higher under the Glu-lim condition than under the N-lim condition, which may explain the stronger regulatory effects of Ino2 on targets under the Glu-lim condition (14).

As we could see few TF-bound genes that have been strongly affected by the deletion of a TF when using a strict cutoff of $|\log_2(FC)|$ of >1 (FC stands for fold change) to define differentially expressed genes, we performed a *t* test to examine whether the bound genes for each TF had an altered expression or not. We used a two-sided *t* test (is there a difference between the bound genes and the nonbound genes in expression profiles), one-sided up *t* test (are the bound genes upregulated compared to the nonbound genes), and one-sided down *t* test (are the bound genes downregulated compared to the nonbound genes). We integrated TF deletion data for Ino2 and Ino4 from reference 14, Oaf1 and Pip2 from reference 21, and Hap1 from reference 31 (these studies used cultivation conditions similar to those used in this study). When a two-sided *t* test was used, some TFs showed significance. However, when splitting the TF deletion data into upregulated or downregulated genes in one-sided *t* tests, we found that for all TFs, the general trend was significant for downregulated genes and some showed significance for upregulated genes as well. The only exception was Hap1 under anaerobic conditions which was significant only for upregulated genes. This is consistent with the previous finding that Hap1 acts as a transcriptional repressor under

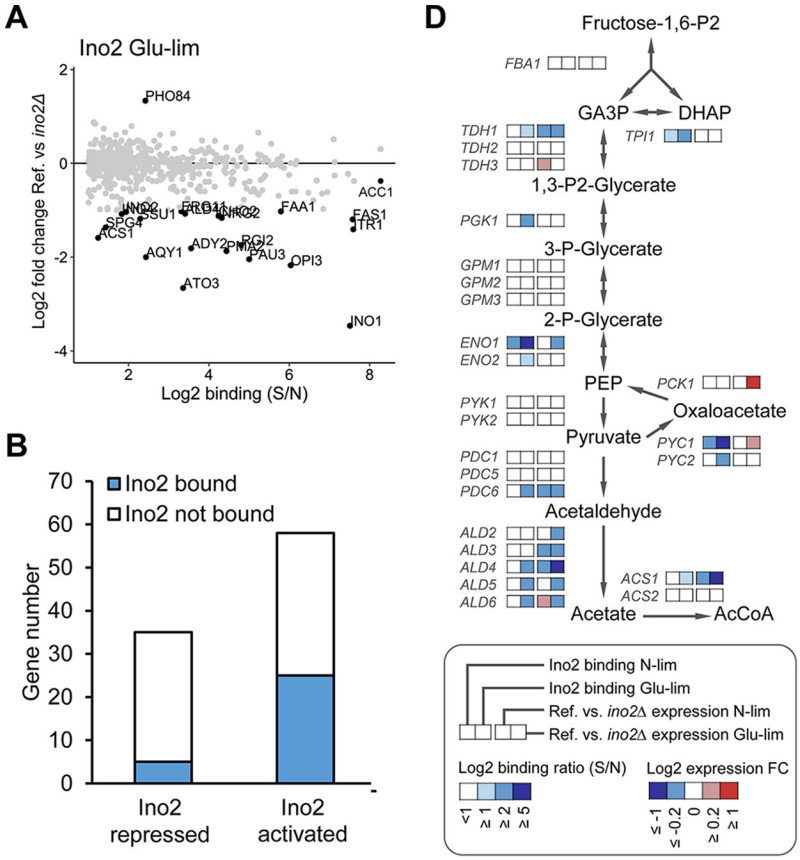

C

TF	Condition	Two-sided	One-sided Down	One-sided Up
Ino2	Glu-lim	0	0	0.00081
Ino2	N-lim	0.00423	0.00033	0.24424
Ino4	Glu-lim	0	0.00022	0.02047
Ino4	N-lim	0	0.00002	0.64716
Hap1	Aerobic	0.331	0.00025	0.00225
Hap1	Anaerobic	0.0333	0.05372	0.00937
Oaf1	Glu-lim	0.09453	0.00076	0.58461
Pip2	Glu-lim	0.00079	0.00592	0.98412

FIG 6 Data integration for elucidating the regulatory effect of TFs on their targets. (A) Effect of *INO2* deletion on the expression of Ino2-binding targets in Glu-lim chemostat culture. The binding ratio (*S*/*N*) of Ino2 determined by ChIP-exo (*x* axis) and the fold change (FC) in the level of expression in the *ino2*Δ deletion mutant relative to the level of expression in the reference strain determined by transcriptome analysis (*y* axis) are shown for each gene. Genes with a $|\log_2(FC)|$ of >1 are highlighted. (B) Distinguishing direct targets from indirect targets within Ino2-dependent genes in Glu-lim chemostat culture. The Ino2-repressed and -activated targets indicate genes showing significant up- and downregulation (adjusted *P* value of <0.05), respectively, in the *ino2*Δ mutant strain relative to the reference strain. (C) *P* values from the *t* test of the five TFs under different conditions showed that in a one-sided *t* test, all TFs had significant ($P < 0.01$) down- or upregulation of genes that were bound compared to nonbound genes. Test results with a *P* value of <0.01 are shown on a gray background. References for the transcriptome data: Ino2 and Ino4 (14), Oaf1 and Pip2 (21), and Hap1 (31). (D) Identification of genes encoding components involved in central carbon metabolism as direct targets of Ino2. The binding ratio (*S*/*N*) of Ino2 and the fold change in the level of expression in the *ino2*Δ mutant strain relative to the level of expression in the reference strain in N-lim and Glu-lim chemostat cultures are shown. Abbreviations: Fructose-1,6-P2, Fructose-1,6-bisphosphate; GA3P, glyceraldehyde 3-phosphate; DHAP, dihydroxyacetone phosphate; PEP, phosphoenolpyruvate; AcCoA, acetyl-CoA.

anaerobic conditions (31). The resulting *t* test table can be seen in Fig. 6D, and the individual plots of FC and $\log_2(S/N)$ can be seen in Fig. S8.

Ino2 and Ino4 are known to directly activate the transcription of several genes encoding components involved in central carbon metabolism, such as the enolase

gene *ENO1* (32) and the AcCoA synthetase gene *ACS2* (33). Through data integration, we found more genes in central carbon metabolism as regulated targets of Ino2, including *TDH1*, *PDC6*, and three aldehyde dehydrogenase genes (Fig. 6C). Aldehyde dehydrogenases are responsible for converting acetaldehyde to acetate, which is on the primary pathway for AcCoA synthesis in *S. cerevisiae* (34). The coregulation of AcCoA and fatty acid biosynthetic genes highlights the importance of coordinating AcCoA supply with lipid biosynthesis (35).

To validate functional outcomes of our TF-binding data, we also constructed an *OAF1* deletion strain. Our data show that Oaf1 has a hierarchical role over some transcription factors, especially as it binds to the promoters of both Pip2 and Adr1 which also regulate fatty acid utilization. Another target of Oaf1 and Pip2 is *ELO1* which encodes the first elongase in fatty acid synthesis. If Oaf1 is controlling expression of *ELO1*, one would expect a decrease in long- and very-long-chain fatty acids, as *ELO1* elongates C_{14} to C_{16} species to C_{18} species (36). Fatty acids were extracted from the *oaf1*Δ strain, and we found that the strain does indeed have higher levels of shorter chains of fatty acids and low levels of longer-chain fatty acids (Fig. S8), which indicates that Oaf1 has a regulatory role over *ELO1*.

DISCUSSION

Knowledge of the structure and function of the transcriptional regulatory network is important for understanding and engineering cellular processes (1, 37). Although considerable data have been accumulated on the regulatory interactions between TFs and their targets in *S. cerevisiae* (38), reconstruction of the transcriptional regulatory network is still challenging owing to the complexity of the network and the limitation of experimental techniques. Identifying direct binding sites is critical for elucidating the hierarchical structure of the regulatory network of TFs because doing so can distinguish direct and indirect targets. Here, we mapped the genome-wide binding targets of five TFs in *S. cerevisiae* using ChIP-exo, with a focus on the regulation of lipid metabolism. By using chemostat cultures, it was possible to examine the relationship between environmental conditions and TF behavior at a constant specific growth rate. As shown in Fig. 1, the advanced resolution of ChIP-exo compared with early ChIP methods enabled us to experimentally determine the distribution of multiple *cis*-acting elements across the genome. The result provides an *in vivo* picture of promoter structure, which could be the basis for precise engineering of promoters in response to specific conditions (39).

Previous studies of the five TFs investigated here mainly focused on their responses to specific environmental signals, such as inositol concentration, which affects the functions of Ino2 and Ino4 (40), and the presence of exogenous oleate, which activates Oaf1 (41). Under industrial cultivation conditions, *S. cerevisiae* is often exposed to changes in the species and concentration of carbon sources as well as dissolved oxygen levels. This motivated us to use four cultivation conditions representing these industrial growth conditions to compare the binding characteristics of the TFs. The results suggest that the binding of these TFs to the genome can be affected by factors other than their well-known specific signals. For example, the intracellular levels of phosphatidic acid, which acts as a central signal in the regulation of Ino2 and Ino4 activity (42), are similar between N-lim and Glu-lim conditions when high concentrations of inositol are present in the culture we used (43). However, the binding target set and regulatory effect of Ino2 are still quite different for the various conditions (see Fig. S7 in the supplemental material). Similar results were observed for Hap1, whose binding targets are different across the three aerobically growing conditions, although they have similar dissolved oxygen levels. We further found that the effect of metabolic status on TF binding could possibly be attributed to changes in chromatin accessibility resulting from the condition-dependent binding of other TFs, which can recruit chromatin remodelers (44). Exploring the causal relationship between chromatin remodeling and the binding of TFs would provide new understanding about the complex process of transcriptional regulation in eukaryotes.

The surprisingly high number of binding targets, together with the significant overlap of targets between the TFs, raises the question of whether all binding is functional. Through the integration of binding data and TF-dependent gene expression data, the contribution of TF binding to the corresponding gene's transcription level was assessed. There is poor overlap between the binding targets and differentially expressed genes as classically defined, but by allowing all genes and all targets to be integrated in the analysis, we could find statistical significance for changes in expression. The data showed that the affected overall binding targets of the deleted TF were in fact downregulated and in one case upregulated. However, at the gene level, we could not see which targets would be most affected by said deletion or if they would be down- or upregulated. Looking at some individual TFs, we can see that for Ino2, there are more than 800 targets in our ChIP-exo data but only 20 genes were substantially affected in the deletion strain; it is therefore difficult to evaluate the regulation directly. Because Ino2 does efficiently regulate the expression of some targets (e.g., *INO1* under Glu-lim condition [Fig. 6A]), we believe the nonfunctional or less functional binding events observed under the same condition are due to not only the low transcriptional activation ability of Ino2 and Ino4 in the presence of exogenous inositol (45) but also the complex internal transcriptional regulatory loop and coregulation of genes by multiple TFs. The cumulative regulation mechanism has been supported by a previous study on *ENO1* expression, where a single gene deletion of the bound TFs each led to decreased but not abolished gene expression from the *ENO1* promoter (32). This is due to the fact that the remaining transcription factors can adapt to the deletion of one TF. Therefore, deletion of a TF may not result in the identification of true functional targets but rather the state of how well the cell is adapting. If, however, the TF is the sole activator/repressor of a gene or in a hierarchical position toward other TFs that are regulating the said gene, then the expression level of the gene might have a correlation with the function of the TF. These results highlight the importance of systematically mapping the binding sites of all TFs in the reconstruction of a genome-scale transcriptional regulatory network.

The emerging computer-assisted tools for pattern recognition using neural networks and deep learning algorithms may allow for better motif discovery (46–48) and help reveal the interplay of TFs on promoters. As we are starting to see highly dynamic and complex regulatory networks in eukaryal cells, such deep learning techniques could lead to the discovery and understanding of regulatory and condition-responsive elements rather than the hierarchical individual TF regulation and thus identify holistic transcriptional regulatory networks that are at the core of molecular biology.

MATERIALS AND METHODS

Strains. The TF-tagging strains were constructed by transforming the uracil auxotrophic strain CEN.PK 113-5D of *Saccharomyces cerevisiae* (49) with a tagging cassette containing the tandem affinity purification (TAP) tag CBP-ProtA coding sequence and *Kluyveromyces lactis URA3* marker gene flanked by 45-bp sequences for homologous recombination at the TF gene locus (50). This integration allows the tag to be fused in-frame to the C-terminal end of each TF connected by a six-glycine linker. Transformants were screened on synthetic complete medium lacking uracil (SC_Ura; Formedium), and the correct integrations were identified by PCR. The function of the TAP tag was confirmed by ChIP followed by quantitative PCR (ChIP-qPCR) of known target promoters. All primers for cassette construction, PCR identification, and ChIP-qPCR are listed in Table S6 in Data Set S1 in the supplemental material. Transcriptome sequencing (RNA-seq) was performed on strain CEN.PK 113-5D complemented by *URA3* as well as a *HAP1*-TAP-tagged strain in all four chemostat conditions, where no significant changes could be identified between the two strains (unpublished data).

Media and cultivations. Single colonies from fresh agar plates were inoculated into 50 ml yeast extract-peptone-dextrose (YPD) medium in shaking flasks and grown for 12 to 24 h. Cells were harvested by centrifugation and resuspended in sterile water to obtain inoculum. Chemostat cultivation in liquid medium with a working volume of 500 ml was carried out using 1.2-liter DASGIP fermentors operated at 30°C with a dilution rate of 0.1 h^{-1}. The pH was maintained at pH 5.0 using 2 M KOH. Minimal medium containing vitamin (1,000× stock solution [all amounts shown for 1 liter]; 0.05 g biotin, 0.2 g 4-aminobenzoic acid, 1 g nicotinic acid, 1 g calcium pantothenate, 1 g pyridoxine-HCl, 1 g thiamine-HCl, and 25 g *myo*-inositol) and trace metal (1,000× stock solution [all amounts shown for 1 liter]: 15.0 g EDTA-Na_2, 4.5 g $ZnSO_4 \cdot 7H_2O$, 0.84 g $MnCl_2 \cdot 2H_2O$, 0.3 g $CoCl_2 \cdot 6H_2O$, 0.3 g $CuSO_4 \cdot 5H_2O$, 0.4 g

$Na_2MoO_4 \cdot 2H_2O$, 4.5 g $CaCl_2 \cdot 2H_2O$, 3 g $FeSO_4 \cdot 7H_2O$, 1 g H_3BO_3, and 0.1 g KI) (51) as well as the following compounds (all amounts shown for 1 liter) were used for feeding: (i) for nitrogen-limited media, 1 g $(NH_4)_2SO_4$, 5.3 g K_2SO_4, 3 g KH_2PO_4, 0.5 g $MgSO_4 \cdot 7H_2O$, 60 g glucose; (ii) for glucose-limited media, 5 g $(NH_4)_2SO_4$, 3 g KH_2PO_4, 0.5 g $MgSO_4 \cdot 7H_2O$, and 7.5 g glucose; (iii) for oxygen- and glucose-limited media, 5 g $(NH_4)_2SO_4$, 3 g KH_2PO_4, 0.5 g $MgSO_4 \cdot 7H_2O$, 7.5 g glucose, 420 mg Tween 80, and 10 mg ergosterol; (iv) for ethanol-limited media, 5 g $(NH_4)_2SO_4$, 3 g KH_2PO_4, 0.5 g $MgSO_4 \cdot 7H_2O$, and 5 g ethanol.

Antifoam 204 at 0.05 ml liter^{-1} (aerobic cultures) or 0.2 ml liter^{-1} (Ox,Glu-lim culture) was added to the feeding media. For aerobic cultures, airflow of 30 liters h^{-1} and stirring speed of 600 rpm (Glu- and N-lim cultures) or 800 rpm (Et-lim culture) were used to keep the dissolved oxygen above 30% of air saturation. For Ox,Glu-lim culture, the fermentor was sparged with 30 liters h^{-1} of nitrogen gas with a stirring speed of 300 rpm. The oxygen and carbon dioxide in the off-gas were measured using the DASGIP GA4 exhaust analyzer after being cooled by a condenser operated at 4°C.

ChIP-exo. Cells cultivated in chemostats were sampled for ChIP-exo analysis after steady state was achieved (optical density at 600 nm [OD_{600}], dissolved oxygen, and off-gas profiles became constant) for 48 to 60 h. Formaldehyde at a final concentration of 1% (wt/vol) and distilled water were added to the cultures to cross-link protein-DNA complexes at an OD_{600} of 1.0 and a total volume of 100 ml. Cross-linking was performed for 12 min at room temperature with shaking followed by quenching, washing, and freezing as previously described (10). ChIP-exo was performed according to a previously reported method (52) with modifications (10, 29). The first adapters contain unique 6-bp index sequences. The final DNA samples were pooled in equimolar amounts and sequenced on the NextSeq 500 system (2 × 75 bp, mid-output mode; Illumina). The ChIP-exo experiments were performed in biological duplicate. All adapters and primers used in the ChIP-exo are listed in Table S7 in Data Set S1.

ChIP-exo data analysis was performed as previously described (10). Briefly, sequencing reads were mapped to reference genome assembly R64-2-1 of *S. cerevisiae* S288C with Bowtie2 (53), and the generated SAM files were converted to sorted BAM files via the removal of low-quality reads. The BAM files were trimmed 70 bases from the 3′ end using trimBam (http://genome.sph.umich.edu/wiki/BamUtil:_trimBam) to increase the resolution. The Integrative Genomics Viewer (IGV) browser (54) was used to visualize the alignment of reads to the genome. The program GEM (20) was used to identify peaks and compare biological duplicates. The noise level was calculated from averaged noise throughout each replicate. Binding events with $\log_2(S/N)$ ratios of >1 are considered to be reliable, where earlier studies on Chip-exo data have used a $\log_2(S/N)$ of >1.5 (29), although with the preprocessing of data, some positive events can be lost (Fig. S3). Identification of target genes was done with the *closest* function of BEDTools (55). Gene targets with a distance of more than 1,200 bp from the binding event center were sorted out. The MEME algorithm (56) was used to identify the consensus motifs for all TFs under all conditions. Forty-base-pair sequences were used as input, and the output motifs should have a length between 6 and 15 bp.

To generate the target gene-based ChIP-exo data tables and heat map of binding profiles, we used MatLab (57). The heat map binding profiles were created by extracting the counts of reads 300 bp up- and downstream of the identified binding site. The counts were $\log_{10}$ transformed, and the data were then transformed into a heat map profile. All heat map profiles were aligned to center binding.

Accession number(s). The ChIP-exo data have been deposited in the Gene Expression Omnibus database under accession number GSE88941.

Data availability. Data are also available for viewing at the UCSC Genome Browser.

SUPPLEMENTAL MATERIAL

Supplemental material for this article may be found at https://doi.org/10.1128/mSystems.00215-17.

FIG S1, TIF file, 3.1 MB.
FIG S2, TIF file, 1.4 MB.
FIG S3, TIF file, 0.5 MB.
FIG S4, TIF file, 1.3 MB.
FIG S5, TIF file, 1.1 MB.
FIG S6, TIF file, 2.8 MB.
FIG S7, TIF file, 2.9 MB.
FIG S8, TIF file, 1.3 MB.
FIG S9, TIF file, 0.5 MB.
DATA SET S1, XLSX file, 1 MB.

ACKNOWLEDGMENTS

This work was supported by the Novo Nordisk Foundation and the Knut and Alice Wallenberg Foundation. The computations were performed on resources at the Chalmers Centre for Computational Science and Engineering (C3SE) provided by the Swedish National Infrastructure for Computing (SNIC).

We declare that we have no conflicts of interest.

REFERENCES

1. Hughes TR, de Boer CG. 2013. Mapping yeast transcriptional networks. Genetics 195:9–36. https://doi.org/10.1534/genetics.113.153262.
2. Fang X, Sastry A, Mih N, Kim D, Tan J, Yurkovich JT, Lloyd CJ, Gao Y, Yang L, Palsson BO. 2017. Global transcriptional regulatory network for Escherichia coli robustly connects gene expression to transcription factor activities. Proc Natl Acad Sci U S A 114:10286–10291. https://doi.org/10.1073/pnas.1702581114.
3. Guzmán-Vargas L, Santillán M. 2008. Comparative analysis of the transcription-factor gene regulatory networks of E. coli and S. cerevisiae. BMC Syst Biol 2:13. https://doi.org/10.1186/1752-0509-2-13.
4. Leyn SA, Kazanov MD, Sernova NV, Ermakova EO, Novichkov PS, Rodionov DA. 2013. Genomic reconstruction of the transcriptional regulatory network in Bacillus subtilis. J Bacteriol 195:2463–2473. https://doi.org/10.1128/JB.00140-13.
5. Österlund T, Bordel S, Nielsen J. 2015. Controllability analysis of transcriptional regulatory networks reveals circular control patterns among transcription factors. Integr Biol 7:560–568. https://doi.org/10.1039/c4ib00247d.
6. Gitter A, Siegfried Z, Klutstein M, Fornes O, Oliva B, Simon I, Bar-Joseph Z. 2009. Backup in gene regulatory networks explains differences between binding and knockout results. Mol Syst Biol 5:276. https://doi.org/10.1038/msb.2009.33.
7. Rhee HS, Pugh BF. 2011. Comprehensive genome-wide protein-DNA interactions detected at single-nucleotide resolution. Cell 147:1408–1419. https://doi.org/10.1016/j.cell.2011.11.013.
8. Lee TI, Rinaldi NJ, Robert F, Odom DT, Bar-Joseph Z, Gerber GK, Hannett NM, Harbison CT, Thompson CM, Simon I, Zeitlinger J, Jennings EG, Murray HL, Gordon DB, Ren B, Wyrick JJ, Tagne J-B, Volkert TL, Fraenkel E, Gifford DK, Young RA. 2002. Transcriptional regulatory networks in *Saccharomyces cerevisiae*. Science 298:799–804. https://doi.org/10.1126/science.1075090.
9. Harbison CT, Gordon DB, Lee TI, Rinaldi NJ, Macisaac KD, Danford TW, Hannett NM, Tagne J-B, Reynolds DB, Yoo J, Jennings EG, Zeitlinger J, Pokholok DK, Kellis M, Rolfe PA, Takusagawa KT, Lander ES, Gifford DK, Fraenkel E, Young RA. 2004. Transcriptional regulatory code of a eukaryotic genome. Nature 431:99–104. https://doi.org/10.1038/nature02800.
10. Liu G, Bergenholm D, Nielsen J. 2016. Genome-wide mapping of binding sites reveals multiple biological functions of the transcription factor Cst6p in Saccharomyces cerevisiae. mBio 7:e00559-16. https://doi.org/10.1128/mBio.00559-16.
11. Henry SA, Kohlwein SD, Carman GM. 2012. Metabolism and regulation of glycerolipids in the yeast Saccharomyces cerevisiae. Genetics 190:317–349. https://doi.org/10.1534/genetics.111.130286.
12. de Boer CG, Hughes TR. 2012. YeTFaSCo: a database of evaluated yeast transcription factor sequence specificities. Nucleic Acids Res 40:D169–D179. https://doi.org/10.1093/nar/gkr993.
13. Carman GM, Henry SA. 1989. Phospholipid biosynthesis in yeast. Annu Rev Biochem 58:635–669. https://doi.org/10.1146/annurev.bi.58.070189.003223.
14. Chumnanpuen P, Nookaew I, Nielsen J. 2013. Integrated analysis, transcriptome-lipidome, reveals the effects of INO- level (INO2 and INO4) on lipid metabolism in yeast. BMC Syst Biol 7:S7. https://doi.org/10.1186/1752-0509-7-S3-S7.
15. Kwast KE, Burke PV, Poyton RO. 1998. Oxygen sensing and the transcriptional regulation of oxygen-responsive genes in yeast. J Exp Biol 201:1177–1195.
16. Gordân R, Murphy KF, McCord RP, Zhu C, Vedenko A, Bulyk ML. 2011. Curated collection of yeast transcription factor DNA binding specificity data reveals novel structural and gene regulatory insights. Genome Biol 12:R125. https://doi.org/10.1186/gb-2011-12-12-r125.
17. Baumgartner U, Hamilton B, Piskacek M, Ruis H, Rottensteiner H. 1999. Functional analysis of the Zn2Cys6 transcription factors Oaf1p and Pip2p: different roles in fatty acid induction of β-oxidation in Saccharomyces cerevisiae. J Biol Chem 274:22208–22216. https://doi.org/10.1074/jbc.274.32.22208.
18. Trzcinska-Danielewicz J, Ishikawa T, Miciałkiewicz A, Fronk J. 2008. Yeast transcription factor Oaf1 forms homodimer and induces some oleate-responsive genes in absence of Pip2. Biochem Biophys Res Commun 374:763–766. https://doi.org/10.1016/j.bbrc.2008.07.105.
19. Rottensteiner H, Hartig A, Hamilton B, Ruis H, Erdmann R, Gurvitz A. 2003. Saccharomyces cerevisiae Pip2p–Oaf1p regulates PEX25 transcription through an adenine-less ORE. Eur J Biochem 270:2013–2022. https://doi.org/10.1046/j.1432-1033.2003.03575.x.
20. Guo Y, Mahony S, Gifford DK. 2012. High resolution genome wide binding event finding and motif discovery reveals transcription factor spatial binding constraints. PLoS Comput Biol 8:e1002638. https://doi.org/10.1371/journal.pcbi.1002638.
21. Smith JJ, Ramsey SA, Marelli M, Marzolf B, Hwang D, Saleem RA, Rachubinski RA, Aitchison JD. 2007. Transcriptional responses to fatty acid are coordinated by combinatorial control. Mol Syst Biol 3:115. https://doi.org/10.1038/msb4100157.
22. Karpichev IV, Small GM. 1998. Global regulatory functions of Oaf1p and Pip2p (Oaf2p), transcription factors that regulate genes encoding peroxisomal proteins in Saccharomyces cerevisiae. Mol Cell Biol 18:6560–6570. https://doi.org/10.1128/MCB.18.11.6560.
23. Choi J-Y, Stukey J, Hwang S-Y, Martin CE. 1996. Regulatory elements that control transcription activation and unsaturated fatty acid-mediated repression of the Saccharomyces cerevisiae OLE1 gene. J Biol Chem 271:3581–3589. https://doi.org/10.1074/jbc.271.7.3581.
24. Dang W, Sutphin GL, Dorsey JA, Otte GL, Cao K, Perry RM, Wanat JJ, Saviolaki D, Murakami CJ, Tsuchiyama S, Robison B, Gregory BD, Vermeulen M, Shiekhattar R, Johnson FB, Kennedy BK, Kaeberlein M, Berger SL. 2014. Inactivation of yeast Isw2 chromatin remodeling enzyme mimics longevity effect of calorie restriction via induction of genotoxic stress response. Cell Metab 19:952–966. https://doi.org/10.1016/j.cmet.2014.04.004.
25. Väremo L, Nielsen J, Nookaew I. 2013. Enriching the gene set analysis of genome-wide data by incorporating directionality of gene expression and combining statistical hypotheses and methods. Nucleic Acids Res 41:4378–4391. https://doi.org/10.1093/nar/gkt111.
26. Hiltunen JK, Mursula AM, Rottensteiner H, Wierenga RK, Kastaniotis AJ, Gurvitz A. 2003. The biochemistry of peroxisomal β-oxidation in the yeast Saccharomyces cerevisiae. FEMS Microbiol Rev 27:35–64. https://doi.org/10.1016/S0168-6445(03)00017-2.
27. Trotter PJ, Adamson AL, Ghrist AC, Rowe L, Scott LR, Sherman MP, Stites NC, Sun Y, Tawiah-Boateng MA, Tibbetts AS, Wadington MC, West AC. 2005. Mitochondrial transporters involved in oleic acid utilization and glutamate metabolism in yeast. Arch Biochem Biophys 442:21–32. https://doi.org/10.1016/j.abb.2005.07.016.
28. Spivakov M. 2014. Spurious transcription factor binding: non-functional or genetically redundant? Bioessays 36:798–806. https://doi.org/10.1002/bies.201400036.
29. Seo SW, Kim D, Latif H, O'Brien EJ, Szubin R, Palsson BO. 2014. Deciphering Fur transcriptional regulatory network highlights its complex role beyond iron metabolism in Escherichia coli. Nat Commun 5:4910. https://doi.org/10.1038/ncomms5910.
30. Chua G, Morris QD, Sopko R, Robinson MD, Ryan O, Chan ET, Frey BJ, Andrews BJ, Boone C, Hughes TR. 2006. Identifying transcription factor functions and targets by phenotypic activation. Proc Natl Acad Sci U S A 103:12045–12050. https://doi.org/10.1073/pnas.0605140103.
31. Hickman MJ, Winston F. 2007. Heme levels switch the function of Hap1 of Saccharomyces cerevisiae between transcriptional activator and transcriptional repressor. Mol Cell Biol 27:7414–7424. https://doi.org/10.1128/MCB.00887-07.
32. Chen M, Lopes JM. 2007. Multiple basic helix-loop-helix proteins regulate expression of the ENO1 gene of Saccharomyces cerevisiae. Eukaryot Cell 6:786–796. https://doi.org/10.1128/EC.00383-06.
33. Hiesinger M, Wagner C, Schüller HJ. 1997. The acetyl-CoA synthetase gene ACS2 of the yeast Saccharomyces cerevisiae is coregulated with structural genes of fatty acid biosynthesis by the transcriptional activators Ino2p and Ino4p. FEBS Lett 415:16–20. https://doi.org/10.1016/S0014-5793(97)01085-5.
34. Krivoruchko A, Zhang Y, Siewers V, Chen Y, Nielsen J. 2015. Microbial acetyl-CoA metabolism and metabolic engineering. Metab Eng 28:28–42. https://doi.org/10.1016/j.ymben.2014.11.009.
35. Zhou YJ, Buijs NA, Zhu Z, Qin J, Siewers V, Nielsen J. 2016. Production of fatty acid-derived oleochemicals and biofuels by synthetic yeast cell factories. Nat Commun 7:11709. https://doi.org/10.1038/ncomms11709.
36. Toke DA, Martin CE. 1996. Isolation and characterization of a gene affecting fatty acid elongation in Saccharomyces cerevisiae. J Biol Chem 271:18413–18422. https://doi.org/10.1074/jbc.271.31.18413.
37. Feist AM, Herrgård MJ, Thiele I, Reed JL, Palsson BØ. 2009. Reconstruc-

tion of biochemical networks in microorganisms. Nat Rev Microbiol 7:129–143. https://doi.org/10.1038/nrmicro1949.
38. Liu G, Marras A, Nielsen J. 2014. The future of genome-scale modeling of yeast through integration of a transcriptional regulatory network. Quant Biol 2:30–46. https://doi.org/10.1007/s40484-014-0027-5.
39. Rajkumar AS, Liu G, Bergenholm D, Arsovska D, Kristensen M, Nielsen J, Jensen MK, Keasling JD. 2016. Engineering of synthetic, stress-responsive yeast promoters. Nucleic Acids Res 44:e136. https://doi.org/10.1093/nar/gkw553.
40. Jesch SA, Zhao X, Wells MT, Henry SA. 2005. Genome-wide analysis reveals inositol, not choline, as the major effector of Ino2p-Ino4p and unfolded protein response target gene expression in yeast. J Biol Chem 280:9106–9118. https://doi.org/10.1074/jbc.M411770200.
41. Karpichev IV, Durand-Heredia JM, Luo Y, Small GM. 2008. Binding characteristics and regulatory mechanisms of the transcription factors controlling oleate-responsive genes in Saccharomyces cerevisiae. J Biol Chem 283:10264–10275. https://doi.org/10.1074/jbc.M708215200.
42. Loewen CJ, Gaspar ML, Jesch SA, Delon C, Ktistakis NT, Henry SA, Levine TP. 2004. Phospholipid metabolism regulated by a transcription factor sensing phosphatidic acid. Science 304:1644–1647. https://doi.org/10.1126/science.1096083.
43. Chumnanpuen P, Zhang J, Nookaew I, Nielsen J. 2012. Integrated analysis of transcriptome and lipid profiling reveals the co-influences of inositol-choline and Snf1 in controlling lipid biosynthesis in yeast. Mol Genet Genomics 287:541–554. https://doi.org/10.1007/s00438-012-0697-5.
44. Ozonov EA, van Nimwegen E. 2013. Nucleosome free regions in yeast promoters result from competitive binding of transcription factors that interact with chromatin modifiers. PLoS Comput Biol 9:e1003181. https://doi.org/10.1371/journal.pcbi.1003181.
45. Santiago TC, Mamoun CB. 2003. Genome expression analysis in yeast reveals novel transcriptional regulation by inositol and choline and new regulatory functions for Opi1p, Ino2p, and Ino4p. J Biol Chem 278:38723–38730. https://doi.org/10.1074/jbc.M303008200.
46. Lanchantin J, Singh R, Lin Z, Qi Y. 2016. Deep Motif: visualizing genomic sequence classifications. arXiv. https://arxiv.org/abs/1605.01133.
47. Park Y, Kellis M. 2015. Deep learning for regulatory genomics. Nat Biotechnol 33:825–826. https://doi.org/10.1038/nbt.3313.
48. Alipanahi B, Delong A, Weirauch MT, Frey BJ. 2015. Predicting the sequence specificities of DNA- and RNA-binding proteins by deep learning. Nat Biotechnol 33:831–838. https://doi.org/10.1038/nbt.3300.
49. van Dijken JP, Bauer J, Brambilla L, Duboc P, Francois JM, Gancedo C, Giuseppin ML, Heijnen JJ, Hoare M, Lange HC, Madden EA, Niederberger P, Nielsen J, Parrou JL, Petit T, Porro D, Reuss M, van Riel N, Rizzi M, Steensma HY, Verrips CT, Vindeløv J, Pronk JT. 2000. An interlaboratory comparison of physiological and genetic properties of four Saccharomyces cerevisiae strains. Enzyme Microb Technol 26:706–714. https://doi.org/10.1016/S0141-0229(00)00162-9.
50. Puig O, Caspary F, Rigaut G, Rutz B, Bouveret E, Bragado-Nilsson E, Wilm M, Séraphin B. 2001. The tandem affinity purification (TAP) method: a general procedure of protein complex purification. Methods 24:218–229. https://doi.org/10.1006/meth.2001.1183.
51. Verduyn C, Postma E, Scheffers WA, Van Dijken JP. 1992. Effect of benzoic acid on metabolic fluxes in yeasts: a continuous-culture study on the regulation of respiration and alcoholic fermentation. Yeast 8:501–517. https://doi.org/10.1002/yea.320080703.
52. Rhee HS, Pugh BF. 2012. ChIP-exo method for identifying genomic location of DNA-binding proteins with near-single-nucleotide accuracy. Curr Protoc Mol Biol Chapter 21:Unit 21.24. https://doi.org/10.1002/0471142727.mb2124s100.
53. Langmead B, Trapnell C, Pop M, Salzberg SL. 2009. Ultrafast and memory-efficient alignment of short DNA sequences to the human genome. Genome Biol 10:R25–R25. https://doi.org/10.1186/gb-2009-10-3-r25.
54. Thorvaldsdóttir H, Robinson JT, Mesirov JP. 2013. Integrative Genomics Viewer (IGV): high-performance genomics data visualization and exploration. Brief Bioinform 14:178–192. https://doi.org/10.1093/bib/bbs017.
55. Quinlan AR, Hall IM. 2010. BEDTools: a flexible suite of utilities for comparing genomic features. Bioinformatics 26:841–842. https://doi.org/10.1093/bioinformatics/btq033.
56. Bailey TL, Elkan C. 1994. Fitting a mixture model by expectation maximization to discover motifs in biopolymers. Proc Int Conf Intell Syst Mol Biol 2:28–36.
57. MATLAB. 2016. R2014b. MathWorks, Natick, MA.
58. Khoomrung S, Chumnanpuen P, Jansa-ard S, Nookaew I, Nielsen J. 2012. Fast and accurate preparation fatty acid methyl esters by microwave-assisted derivatization in the yeast Saccharomyces cerevisiae. Appl Microbiol Biotechnol 94:1637–1646. https://doi.org/10.1007/s00253-012-4125-x.